AGU PUBLICATIONS

JGR

Journal of Geophysical Research: Oceans

RESEARCH ARTICLE

10.1002/2017JC013086

Wind-Driven Response of the Upper Ocean Along the U.S. West Coast to Tropical MJO Convection

Bradford S. Barrett[1], Alexander R. Davies[1], and Jacob I. Rose[1]

[1]Oceanography Department, U.S. Naval Academy, Annapolis, MD, USA

Abstract In this study, time-lagged composites of OSCAR upper ocean currents from February to May of 1993–2016 were binned by active phase of the leading atmospheric mode of intraseasonal variability, the Madden-Julian Oscillation (MJO). Seven days after the convectively active phase of the MJO is present in the tropical Indian Ocean, anomalously strong south-southeastward upper ocean currents are seen along nearly the entire U.S. west coast. Seven days after the convectively active phase is present in the tropical western Pacific Ocean, upper ocean current anomalies reverse along the U.S. west coast, with weaker southward flow. A physical pathway to the ocean was found for both of these phases: (a) tropical MJO convection modulates upper tropospheric heights and circulation over the Pacific Ocean; (b) those anomalous atmospheric heights adjust the strength and position of the Aleutian Low and Hawaiian High; (c) surface winds change in response to the adjusted atmospheric pressure patterns; and (d) those surface winds project onto upper ocean currents.

Plain Language Summary Thunderstorms in the tropical Indian and Pacific Oceans are found to generate a response in upper ocean currents along the U.S. west coast.

Key Points:
- Intraseasonal convection in the Indian Ocean drives southward acceleration of the California current
- Intraseasonal convection in the western Pacific Ocean drives northward acceleration of the California current
- An atmospheric pathway between the tropics and the extratropics supports the observed ocean variability

Correspondence to:
B. S. Barrett,
bbarrett@usna.edu

Citation:
Barrett, B. S., Davies, A. R., & Rose, J. I. (2017). Wind-driven response of the upper ocean along the U.S. west coast to tropical MJO convection. *Journal of Geophysical Research: Oceans*, *122*, 8196–8207. https://doi.org/10.1002/2017JC013086

Received 10 MAY 2017
Accepted 15 SEP 2017
Accepted article online 21 SEP 2017
Published online 27 OCT 2017

1. Introduction

It is widely recognized that surface wind forcing plays a critical role in driving upper ocean dynamics. Significant advancements have been made in understanding the oceanic response to atmospheric forcing as it relates to both small-scale and large-scale processes. Examples include, but are not limited to, wind-wave generation (Hasselmann et al., 1973; Miles, 1957; Phillips, 1985), wind-generated Langmuir circulation (McWilliams et al., 1997; Weller & Price, 1988), El Niño's impact on the Kuroshio Current (Yamagata, 1985) and the Gulf Stream (Taylor et al., 1998), the Southern Annular Mode's impact on the Antarctic Circumpolar Current (Sallee et al., 2008), and the Pacific Decadal Oscillation's impact on the Kuroshio (Latif & Barnett, 1996; Qiu, 2003) and California currents (Biondi et al., 2001). However, despite this considerable progress, the impact of intraseasonal atmospheric variability on surface ocean dynamics remains relatively understudied and unresolved, particularly in the extratropics and including along the U.S. west coast.

One major mode of atmospheric intraseasonal variability is the Madden-Julian Oscillation (MJO; Madden & Julian, 1971, 1972). In the equatorial Indian and western Pacific Oceans, the MJO is defined by an eastward-moving region of enhanced deep convection and precipitation approximately 10,000 km across and centered in the tropics. On both sides of this region of anomalously enhanced convection are regions of anomalously suppressed convection. These enhanced and suppressed regions are connected by zonal overturning circulations extending through the troposphere. These anomalies of convection and circulation circumnavigate the tropics with a period between approximately 30 and 90 days (Madden & Julian, 1994). One consequence of the MJO convection, and one that is critically important to this current study, is that tropical upper tropospheric diabatic heating, precisely the kind of heating associated with the MJO, can be an efficient Rossby wave source into the extratropics (Ferranti et al., 1990; Wallace & Gutzler, 1981). Hoskins and Karoly (1981), Bladé and Hartmann (1995), Jin and Hoskins (1995), Matthews et al. (2004), and Seo and Son (2012) confirmed this planetary-scale atmospheric Rossby wave train response to MJO and MJO-like upper troposphere heating. Through this connection to global atmospheric circulation, the MJO has been shown to have direct (in the tropics) and indirect (via teleconnections to the extratropics) influences on many weather phenomena, spanning an impressive range of spatial and temporal scales: the

El Niño-Southern Oscillation (Hendon et al., 2007; Kapur & Zhang, 2012; McPhaden, 1999), the North Atlantic Oscillation (Cassou, 2008), the Pacific-North American pattern (Baxter et al., 2014; Baxter & Nigam, 2013), the Southern Annular Mode (Fauchereau et al., 2016; Flatau & Kim, 2013), the South Asian monsoon (Goswami, 2005), tropical cyclone activity in the Atlantic basin (Barrett & Leslie, 2009; Klotzbach & Oliver, 2015), global precipitation (Donald et al., 2006), U.S. tornado activity (Barrett & Gensini, 2013), and surface air quality (Barrett & Raga, 2016; Liu et al., 2015). In the tropics, the modulation from the MJO onto the ocean is local, including a dynamical response in the Indian Ocean to intraseasonal wind variability seen as a spike in power spectra of zonal currents between 30 and 50 days (Han, 2005; Han et al., 2001; Iskandar & McPhaden, 2011; Schott et al., 2009; Sengupta et al., 2007). This ocean response is the result of a dynamical ocean coupling mechanism by which westerly surface winds generate an eastward-propagating Kelvin wave, one that can reflect off Sumatra feed back to subsequent MJO events as they enter the Indian Ocean (Webber et al., 2010). Furthermore, westerly wind bursts associated with the MJO can excite eastward ocean jets in the Indian Ocean that modify sea surface temperatures for several weeks after the MJO passes (Moum et al., 2014). This multiscale projection of the MJO onto both the tropical ocean and the extratropical atmosphere underlies the hypotheses tested in this study, namely that the MJO could modulate upper ocean currents along the U.S. west coast via a modulation of the extratropical atmosphere. In support of that hypothesis, Matthews and Meredith (2004) noted that the MJO can modulate the Southern Annular Mode during southern hemisphere winter, and they found a projection of that atmospheric modulation as an acceleration in the Antarctic circumpolar ocean current at 60°S.

While seasonal variability of ocean currents is well documented across all ocean basins, subseasonal and intraseasonal variability of surface ocean currents in the extratropics is a relatively new area of study. The MJO's in situ impacts on the tropical ocean on the intraseasonal time scale have been well studied (Duvel & Vialard, 2007; Halkides et al., 2015; Jones et al., 1998; Kemball-Cook & Wang, 2001; Maloney & Sobel, 2004; Roundy & Kiladis, 2006; Shinoda et al., 2013; Waliser et al., 2003; Zhang et al., 2010; Zhou & Murtugudde, 2010), and indeed, those air-sea fluxes are fundamental to MJO convection on the intraseasonal time scale (Hendon, 2005; Kang et al., 2013; Seo et al., 2014; Shinoda et al., 2008; Webber et al., 2012; Woolnough et al., 2007). However, connections between the MJO and intraseasonal variability of ocean currents in the subtropics and extratropics remain largely unknown. In one of the studies to explore this relationship, Wang et al. (2013) identified cyclonic and anticyclonic gyres formed from MJO-driven winds in the South China Sea. They concluded that the MJO has an important imprint on the summer climatology of South China Sea circulation and recommended more research to further understand that relationship. In another study, Marshall and Hendon (2014) found that Ekman-induced downwelling along the northwest coast of Australia resulted from local meridional wind anomalies associated with different MJO phases. They noted that downwelling modulated the Leeuwin current, and as a result, they encouraged training for operational forecasters to raise awareness of their newly discovered process. Finally, Liu et al. (2012) documented an upwelling response to MJO-driven winds off the east coast of Vietnam in August 2007.

Despite these studies, there does not appear to be much work to connect the MJO to extratropical upper ocean circulation in the northeastern Pacific Ocean. However, many oceanic features exhibit direct responses to surface wind forcing and potentially on time scales of the MJO. Furthermore, MJO-driven upper troposphere Rossby wave activity has already been identified along the U.S. west coast (Jones & Carvalho, 2014; Matthews et al., 2004; Roundy, 2012; Sakaeda & Roundy, 2015; Sardeshmukh & Hoskins, 1988), and via three-dimensional quasi-geostrophic theory, these MJO-driven Rossby waves will modulate surface pressure systems and surface winds (e.g., Bluestein, 1992). Thus, a physical pathway between the anomalous tropical convection of the MJO and the upper ocean along the U.S. west coast likely exists, and documenting that modulation and identifying phases when it is strongest was the primary objective of this study. The remainder of this paper is organized as follows: data sets and methodologies used in the analysis are described in section 2. Results of the MJO-ocean analysis are presented in section 3. Finally, conclusions from this study and suggestions for future work are offered in section 4.

2. Data and Methods

To establish an atmospheric link between the MJO convection and upper ocean currents along the U.S. west coast, daily 300 hPa heights, 10 m winds, and mean sea level pressures at 0000 UTC from the ERA-

Interim reanalysis (Dee et al., 2011; freely available for download online at http://www.ecmwf.int/en/research/climate-reanalysis/era-interim) were analyzed. The data spanned the period 1980–2016 and were analyzed for the months of February through May. This late winter and early spring time period was chosen to coincide both with greatest MJO intensity (Lafleur et al., 2015) and with the timing of the spring bloom in the California current system (Henson & Thomas, 2007), which is important for fisheries along the Pacific coast of North America. A follow-on study is planned to explore potential biological response to the MJO during these months. Atmospheric heights and mean sea level pressure were analyzed at 2.5° × 2.5° latitude-longitude spacing, while 10 m winds were analyzed at higher resolution (0.125° × 0.125°) to better capture smaller-scale variability close to North America (although it should be noted that the native resolution of the ERA-Interim data set is closer to 0.75° × 0.75°). To consider together the observations from different months, atmospheric variables were converted to standard anomalies by subtracting the corresponding long-term monthly mean from each daily value, and then dividing the resulting anomaly by the long-term monthly standard deviation. Daily standard anomalies were then binned by lagged phase of the MJO, whereby each standard anomaly was binned according the phase of the MJO 7 days prior, following the methodology of Barrett et al. (2015). A 7 day temporal lag was selected following Cassou (2008), L'Heureux and Higgins (2008), Lin and Brunet (2009), and Flatau and Kim (2013), who found that the Northern Hemisphere extratropical atmospheric response lagged MJO convection by approximately 7 days. Converting anomalies to standard anomalies allows for compositing across all four months. MJO amplitude and phase were determined from the Real-time Multivariate MJO (RMM) index (Wheeler & Hendon, 2004; freely available for download online at http://www.bom.gov.au/climate/mjo/), where active MJO was defined as one with an amplitude $(RMM1^2 + RMM2^2)^{0.5}$ greater than or equal to 1.0, and *RMM*1 and *RMM*2 are the two leading principal components that form the index. Standard anomalies 7 days after inactive MJO (amplitude less than 1.0) were not included in the analysis. Finally, statistical significance of the composite standard anomalies for each MJO phase was determined at the 95% confidence level via a Student's *t* test. The *t* statistic was calculated for each atmospheric variable as follows:

$$t_{i,j} = \frac{\bar{x}_{i,j} - \mu_j}{\sigma_j / \sqrt{n_i - 1}}$$

where $\bar{x}_{i,j}$ is the composite anomaly for month *j* 7 days after MJO phase *i*, μ_j and σ_j are the long-term mean and long-term standard deviation for month *j*, and n_i is the number of observations of MJO phase *i*. In this calculation, *i* ranged from 1 to 8 and *j* from February to May.

Ocean currents in the upper 30 m were analyzed from the NASA Ocean Surface Current Analyses Real-time (OSCAR; freely available for download online at ftp://podaac-ftp.jpl.nasa.gov/allData/oscar/preview/L4/oscar_third_deg/) product at one-third degree spatial resolution for the period spanning 1993–2016 and for the months of February through May. Pentad OSCAR *u* and *v* current components were converted to standard anomalies using the same method described above for the atmospheric variables. OSCAR standard anomalies were then binned by lagged MJO phase, whereby each standard anomaly was binned according the phase of the MJO 7 days before the date of the pentad center. Similar to the method for the atmospheric variables, OSCAR pentads that occurred 7 days after inactive MJO (amplitude less than 1.0) were not considered in this study. To remove some of the mesoscale variability in the California current system along the coast, a three-point (one degree), two-dimensional spatial smoother was applied to OSCAR standard anomalies. To focus the analysis to the California current system, only OSCAR standard anomalies within approximately 250 km of the coastline were retained. Finally, similar to the method used for the atmospheric variables, statistical significance of the OSCAR composite standard anomalies for each MJO phase was determined at the 90% and 95% confidence levels using the Student's *t* test.

3. Results

3.1. Monthly Mean Ocean and Atmosphere States

Mean zonal upper ocean currents from February to May vary slightly from month to month, with onshore flow (positive *u*) located along Oregon and Washington in each month, offshore flow (negative *u*) located along northern California in each month, and onshore flow again located along southern California in each month (Figure 1). Mean meridional upper ocean currents from February to May show more month-to-

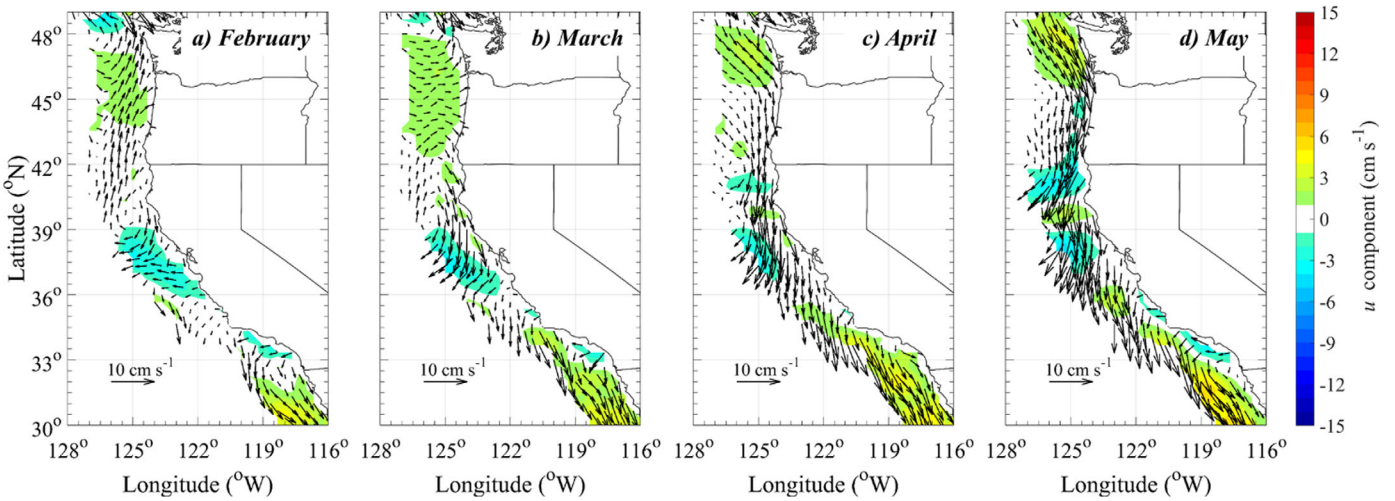

Figure 1. Monthly mean zonal (*u*) OSCAR currents for (a) February, (b) March, (c) April, and (d) May 1993–2016. Vectors show full currents (and a reference length is given for 10 cm s^{-1}); shading represents the zonal component (in cm s^{-1}).

month variability than the zonal currents, particularly from 40°N to 50°N: in February, mean currents in that area are northward (positive *v*), while in May, mean currents in that area reverse to southward (negative *v*) (Figure 2). From 30°S to 40°S, mean meridional currents are primarily southward in all months but intensify as the season progresses (Figure 2). The anomalies presented in the next sections were calculated with respect to these monthly mean states (Figures 1 and 2). It is important to note that the direction and intensity of mean upper ocean currents in each month is similar to mean surface wind direction in those months (Figure 3). That similarity supports the hypothesis of this study that the MJO, which modulates surface winds, would thus project into the upper ocean as well.

3.2. Ocean Response to MJO Convection

Upper ocean currents vary 7 days after active MJO, both in the zonal (Figure 4) and meridional (Figure 5) directions. Indeed, all eight MJO phases, representing anomalous tropical convection spanning from the Indian Ocean eastward to Africa, are associated with statistically significant *u* and *v* ocean current anomalies. Some of the composite *u* and *v* anomalies even exceed ±1 standard deviation from the long-term monthly mean. Additionally, all eight MJO phases feature coherent spatial regions, defined here as regions

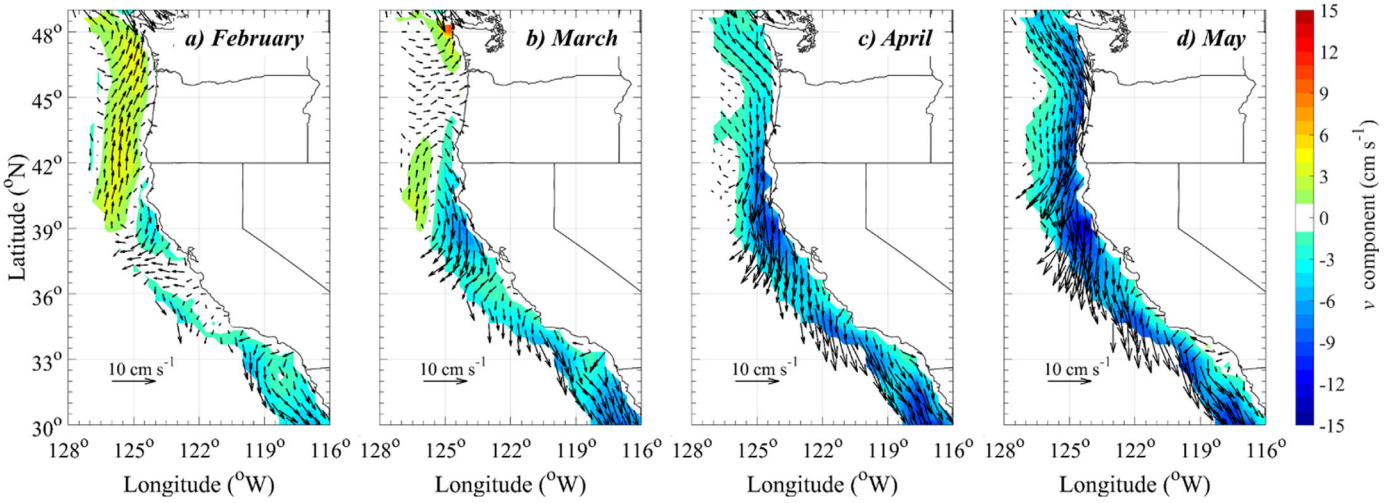

Figure 2. Monthly mean meridional (*v*) OSCAR currents for (a) February, (b) March, (c) April, and (d) May 1993–2016. Vectors show full currents (and a reference length is given for 10 cm s^{-1}); shading represents the meridional component (in cm s^{-1}).

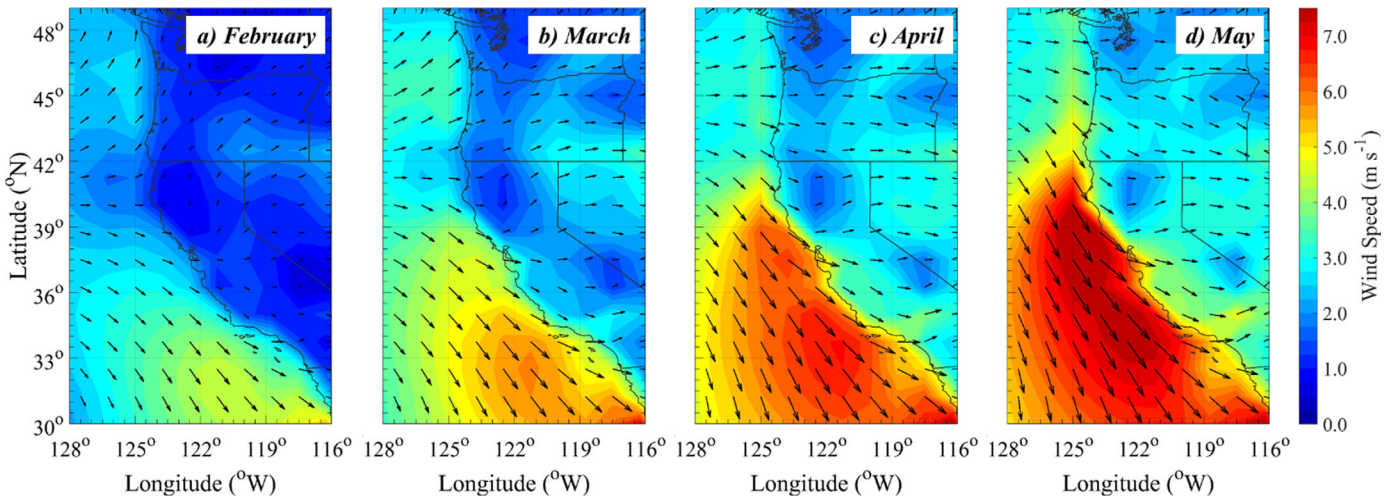

Figure 3. Monthly mean 10 m wind direction (arrows) and speed (color-filled contours, in m s^{-1}) for (a) February, (b) March, (c) April, and (d) May 1980–2016.

with the same anomaly sign and larger than 40,000 km^2 (approximately represented by a 200 km × 200 km region). The presence of those spatially coherent regions suggests that the MJO projects onto synoptic-scale upper ocean processes.

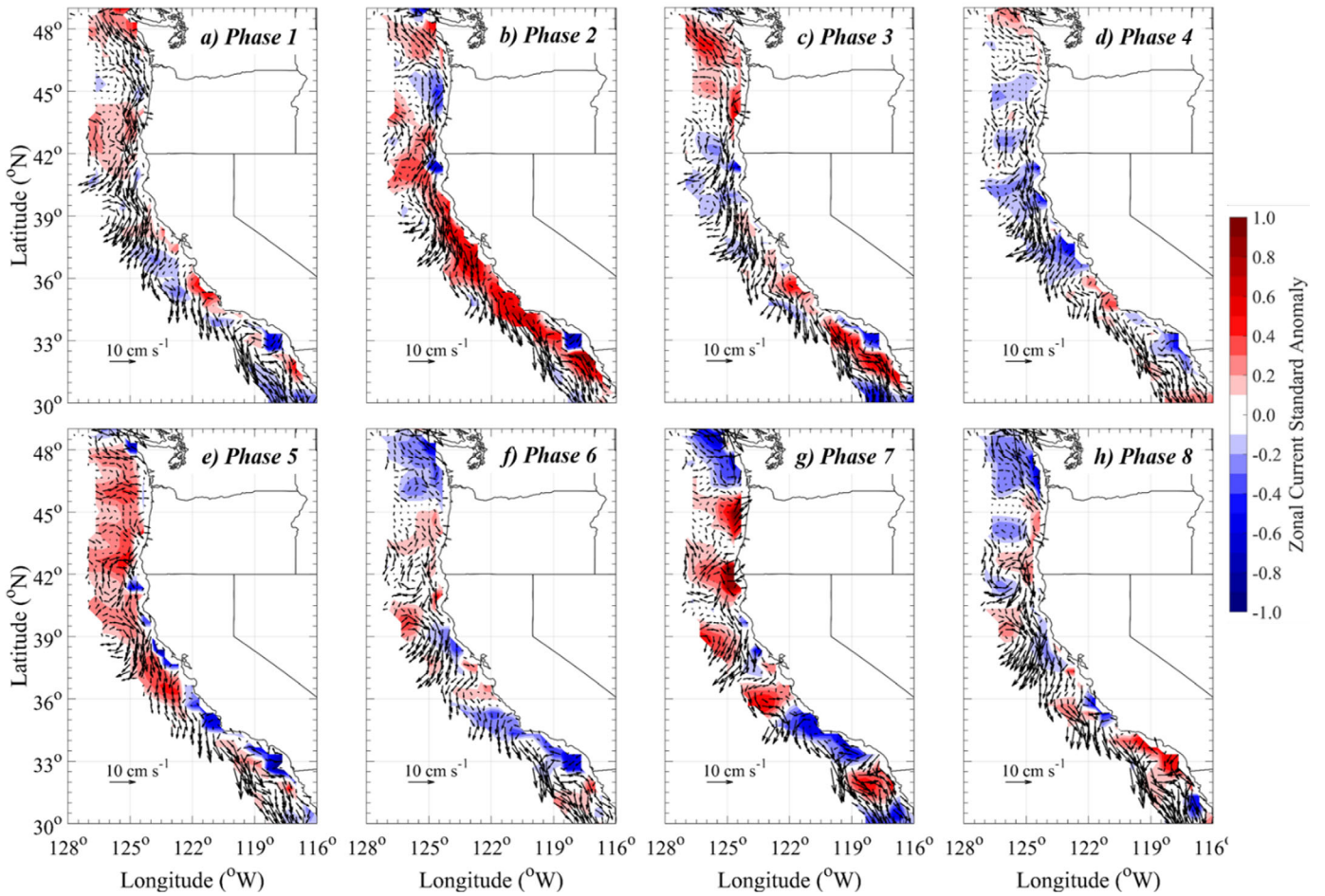

Figure 4. Composite standard anomalies of zonal (*u*) OSCAR currents in the upper ocean for (a–h) MJO Phases 1–8, for February–May 1993–2016 at 7 day time lags. Vectors show mean currents for each phase (and a reference length is given for 10 cm s^{-1}); color shading represents standard anomalies of the zonal component of the current.

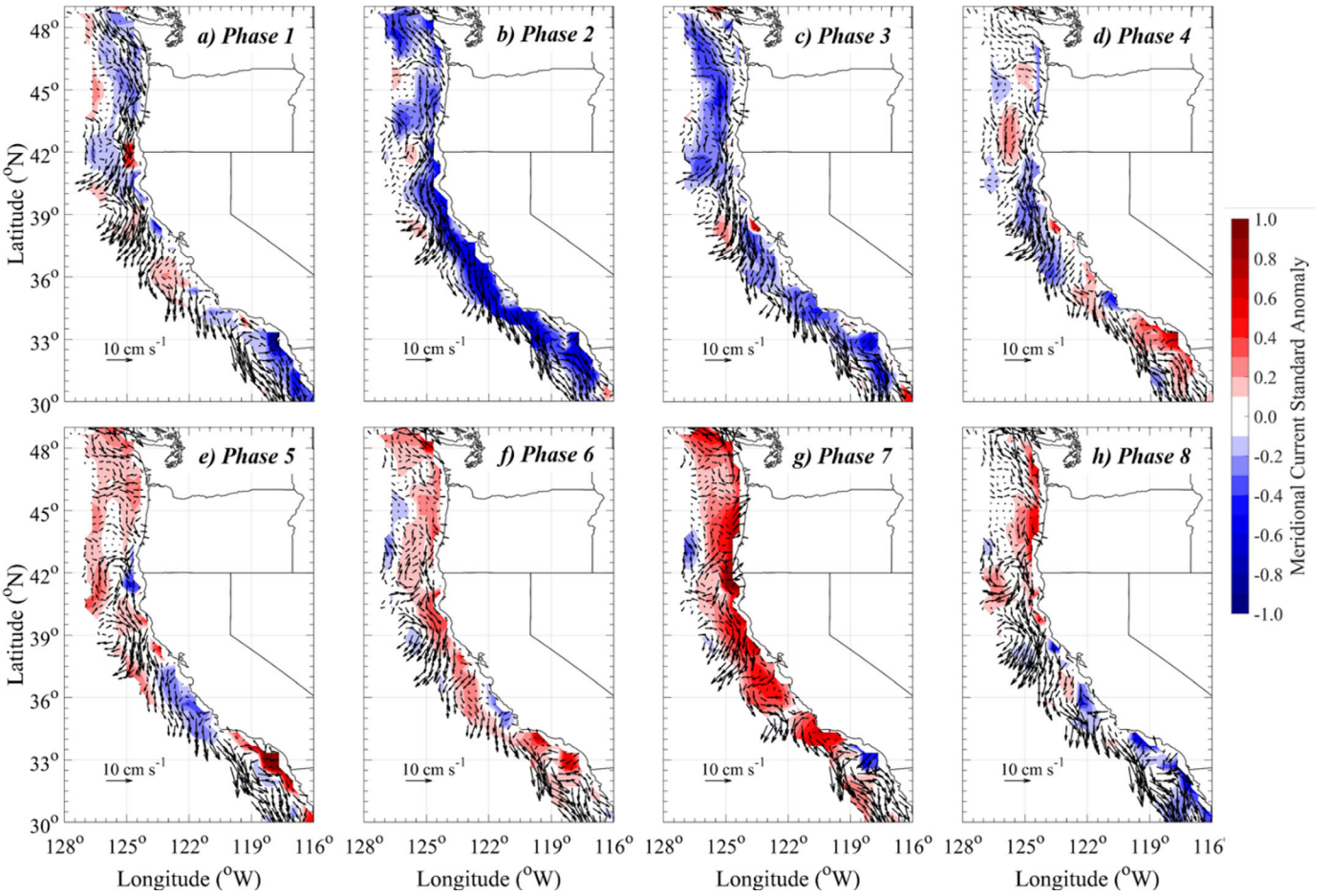

Figure 5. Composite standard anomalies of meridional (*v*) OSCAR currents in the upper ocean for (a–h) MJO Phases 1–8, for February–May 1993–2016 at 7 day time lags. Vectors show mean currents for each phase (and a reference length is given for 10 cm s^{-1}); color shading represents standard anomalies of the meridional component of the current.

In particular, 7 days after Phase 2 (when the convectively active phase is present in the Indian Ocean) and Phase 7 (when the convectively active phase is present in the western Pacific Ocean), anomalies of the *u* (Figures 6a and 6b) and *v* (Figures 6c and 6d) ocean components are strongest in magnitude and show greatest spatial coherence. Those two phases were thus analyzed further, to determine the physical mechanisms responsible for the observed anomalous upper ocean currents along the U.S. west coast.

3.3. Physical Mechanisms for Oceanic Response After Active Convection in the Indian Ocean

Seven days after the convectively active MJO phase is present in the Indian Ocean (MJO Phase 2), anomalous atmospheric 300 hPa heights show ridging east of Japan, centered near 40°N and extending from 210°W to 160°W (Figure 7a). To the south of that anomalous ridging, anomalous troughing is centered near 25°N and extends from 250°W to 160°W (Figure 7a). That anomalous height pattern results in a weakening of the upper tropospheric east Asian Jet, which extends eastward into the north Pacific Ocean. This decelerated east Asian Jet is followed by downstream negative height anomalies over North America (Figure 7a). Via quasi-geostrophic adjustment mechanisms (Carlson, 1991), the 300 hPa atmospheric height anomalies project onto mean sea level pressure (MSLP), yielding an eastward-shifted Aleutian Low and a stronger and southward-shifted and eastward-shifted Hawaiian High (Figure 7c). With the shift in those pressure centers 7 days after MJO Phase 2, faster zonal 10 m winds are located over much of the eastern and central North Pacific, including along the U.S. west coast (Figure 8a). The eastward shift in both the Aleutian Low and the Hawaii High also results in stronger flow in the meridional direction (Figure 8c). Positive *v* wind anomalies, indicating anomalously stronger surface winds from the south, are located along the U.S. west coast from 40°N to 55°N, while negative *v* wind anomalies, indicating anomalously stronger surface winds from the

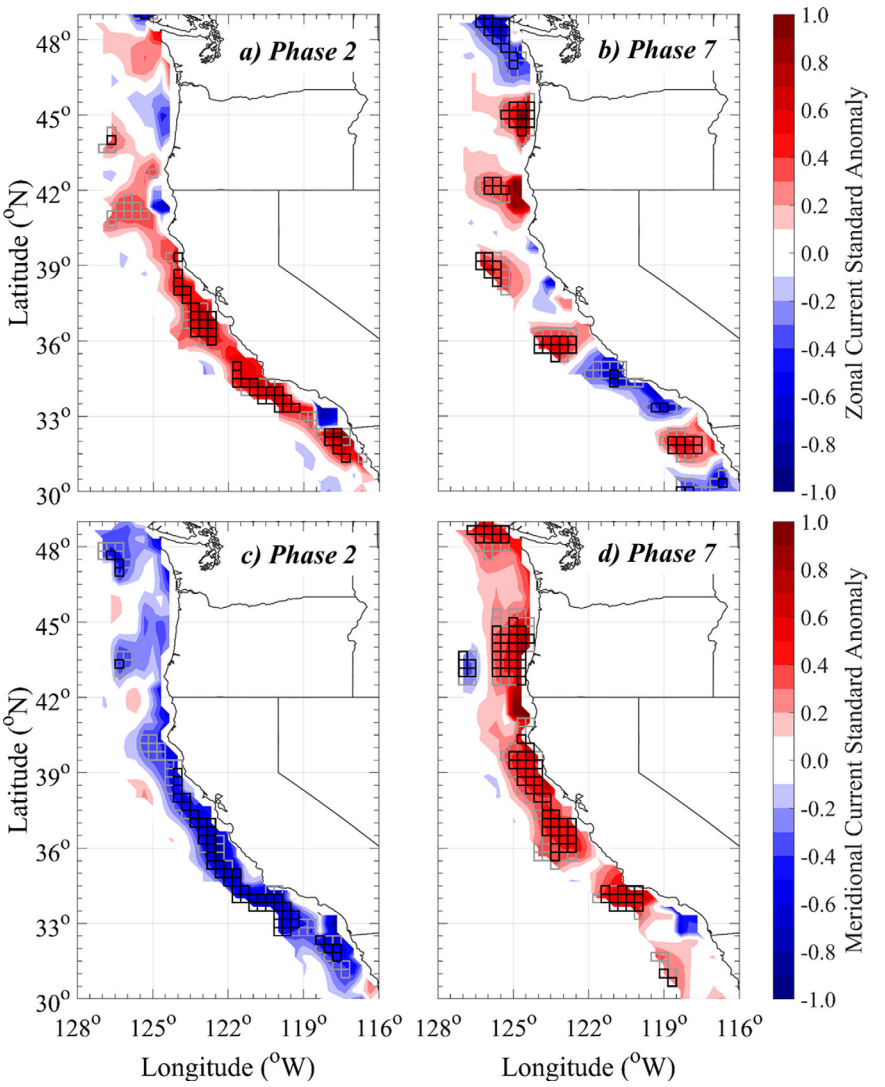

Figure 6. (a, b) Composite standard anomalies of zonal (*u*) and (c, d) meridional (*v*) OSCAR upper ocean currents for MJO Phases (a, c) 2 and (b, d) 7 for February–May 1993–2016 at 7 day time lags. Color shading represents standard anomalies of the respective current component. Black boxes indicate anomalies that were statistically significant at the 95% confidence level; gray boxes indicate anomalies statistically significant at the 90% level.

north, are located along the coast from 25°N to 40°N. Those anomalously strong surface winds project onto currents in the upper ocean, as indicated by the coherent regions of statistically significantly currents in Figures 6a and 6c (i.e. surface currents that are statistically different from the climatological mean state with 95% confidence). For example, positive zonal *u* current anomalies are seen from about 30°N south to 42°N, with standard anomalies up to +0.8 along the central and southern California coast (Figure 6a). Those anomalies represent a stronger eastward component of the upper ocean current in southern California and a deceleration of the westward current in central California (reference the mean state in Figure 1), and they extended from the coast outward over 200 km. Additionally, negative meridional *v* current anomalies are located in the same region, from approximately 30°N to 50°N, and are greatest along the central and southern California coast (Figure 6c). In central and southern California, those anomalies represent an anomalously strong southward mean upper ocean current (Figure 2), and similar to the *u* component, they also extend from the coast outward over 200 km.

3.4. Physical Mechanisms for Oceanic Response After Active Convection in the Western Pacific Ocean

Seven days after the MJO active convective envelope entered the western Pacific Ocean (MJO Phase 7), anomalies in the atmospheric 300 hPa height field tend to take the opposite sign of those observed after

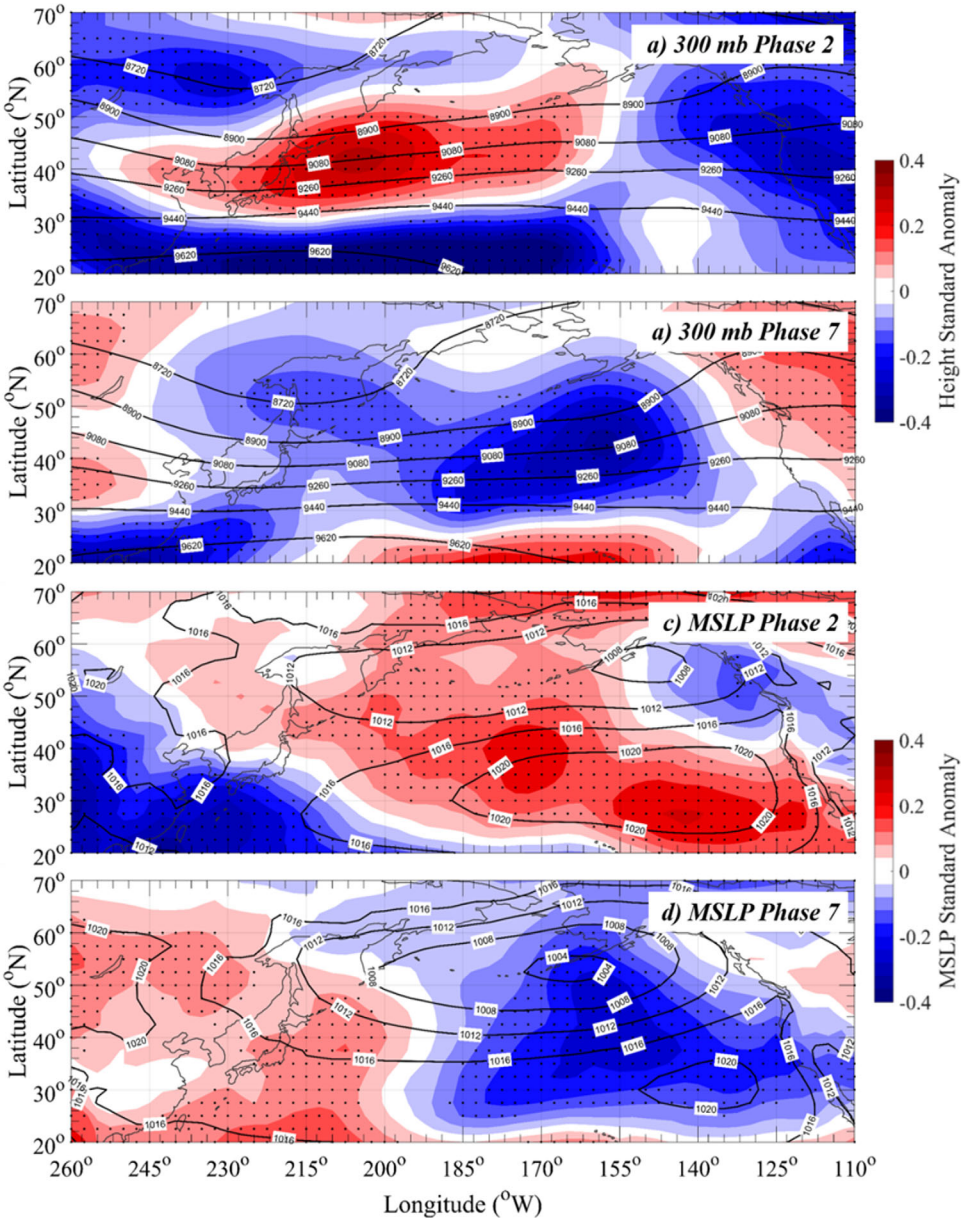

Figure 7. Composite mean (black contours, in m) and standard anomalies (colored; black dot stippling indicates anomalies significant at the 95% confidence level) of 300 hPa height for February–May 1980–2016 for (a) MJO Phase 2 and (b) MJO Phase 7. In (c, d), as in Figures 7a and 7b but for mean sea level pressure (black contours, in hPa).

active convection in the Indian Ocean. Specifically, the climatological trough over the Gulf of Alaska is stronger, with negative 300 hPa height anomalies centered near 45°N, 150°W, while the subtropical ridge near 20°N, 180°W is stronger (Figure 7b). That pattern of 300 hPa height anomalies projects onto the surface to yield a both a stronger and a southwestward-extended Aleutian Low (Figure 7d). Furthermore, the Hawaiian High is weaker and shifted westward compared to its mean position (Figure 7d). That pressure pattern over the eastern North Pacific (east of 135°W) 7 days after MJO Phase 7 results in a broad weakening in the zonal 10 m winds poleward of about 35°N (Figure 8b) and stronger zonal winds equatorward of 30°N. It also yields a broad area of positive *v* wind anomalies from about 45°N to 30°N, along the U.S. coast (Figure 8d). North of 45°N, the climatological surface winds are southerly, and the southwestward shift in the Aleutian Low yields weaker southerly surface winds, seen as negative *v* wind anomalies north of 45°N (Figure 8d), although those anomalies are located over land.

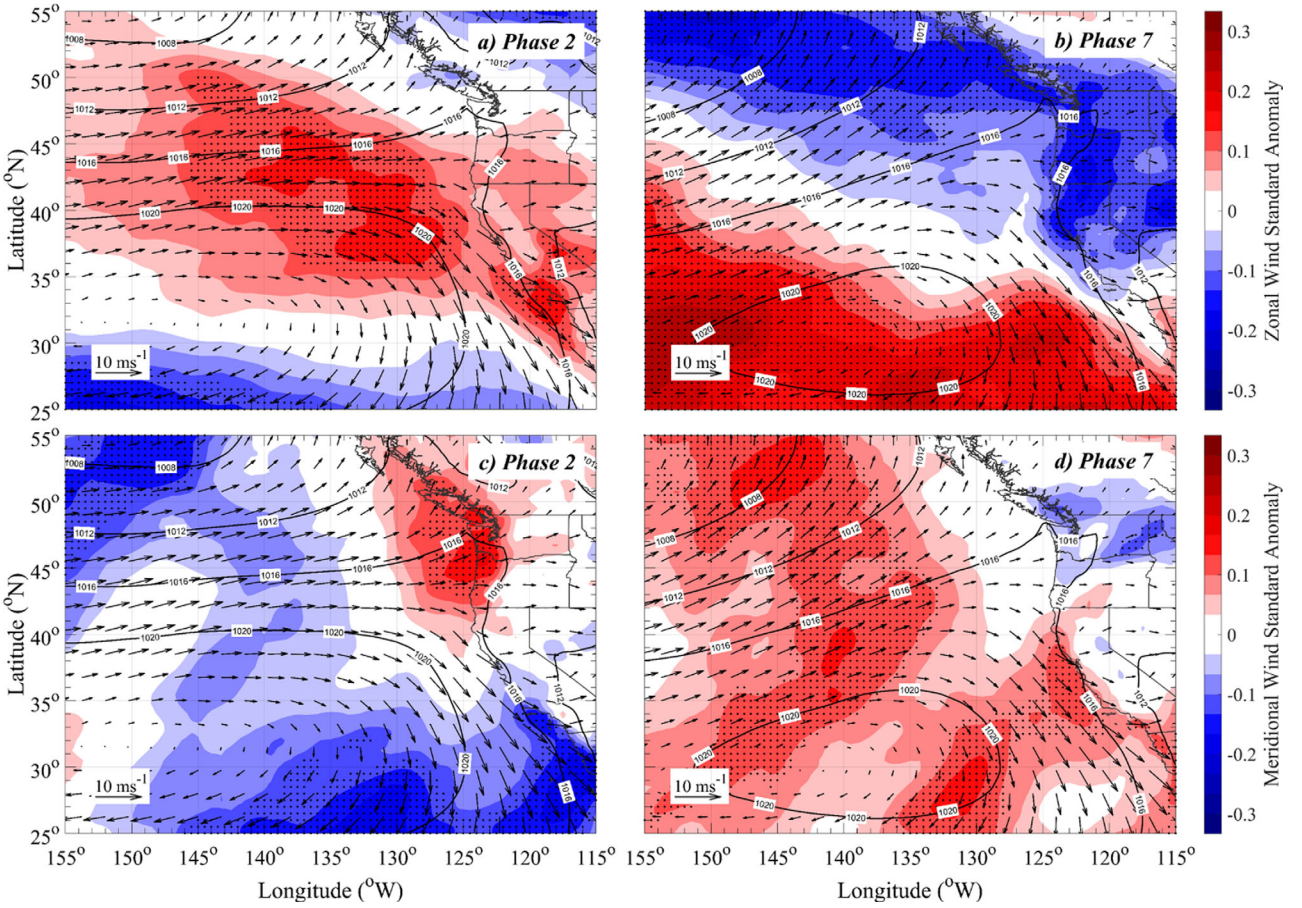

Figure 8. Composite standard anomalies of (a, b) 10 m zonal (*u*) wind components, and (c, d) 10 m meridional (*v*) wind components, for February–May 1980–2016 for (a, c) MJO Phase 2 and (b, d) MJO Phase 7. Vectors show mean winds (and a reference length is given for 10 m s^{-1}); and black dot stippling indicates wind standard anomalies statistically significant at the 95% confidence level. In all figures, composite mean sea level pressures (black contours, in hPa) are overlaid.

Just as is seen after MJO Phase 2, those anomalous surface winds then act to drive ocean current anomalies with coherent regions that are statistically significantly different from the climatological mean state with both 90% and 95% confidence. Because the surface wind anomaly pattern in Phase 7 is largely opposite of the pattern in Phase 2 (compare Figure 8a with 8b, and Figure 8c with 8d), the wind-driven upper ocean anomalies should also have reversed. Indeed, a reversal in the ocean currents is seen (compare Figure 6a with 6b, and Figure 6c with 6d), and the signal is most prominently in the meridional *v* component. In the *v* direction 7 days after Phase 7, current anomalies along nearly the entire U.S. west coast are positive, which is nearly exactly opposite of the anomaly signal seen 7 days after Phase 2. The positive anomalies in Phase 7 indicate a weakening of the climatological southward current along the California coast. In the zonal *u* component, negative anomalies are seen along the southern California coast, and weaker positive anomalies are seen along the northern California coast. Along the Oregon and Washington coasts, those anomalies represent either a weakening of the mean southeastward current (such as in May, when the anomalies are negative) or less of a strengthening of that mean current (such as in February and March, when the anomalies are positive).

4. Conclusions

The primary objective of this study was to test whether upper ocean currents along the U.S. west coast varied 7 days after anomalous atmospheric convection in the tropics during the months of February–May. Statistically significant (at both the 90% and 95% confidence levels) ocean current anomalies were found for all eight MJO phases, in both zonal *u* and meridional *v* components. Time-lagged anomalies after active

convection in two MJO regions, the Indian Ocean and western Pacific Ocean, showed greatest magnitude and the largest spatially coherent regions, particularly in the meridional direction. Furthermore, those ocean anomalies were strongly supported by atmospheric anomalies, with a defined pathway from the tropical atmosphere to the extratropical ocean. For example, in good agreement with Hoskins and Karoly (1981), Bladé and Hartmann (1995), Jin and Hoskins (1995), Matthews et al. (2004), and Seo and Son (2012), the extratropical atmosphere over the Pacific Ocean responds to tropical convection over both the Indian (Phase 2) and western Pacific (Phase 7) Oceans, and that response is manifest in atmospheric height anomalies at 300 hPa 7 days after active MJO convection. Those height anomalies adjust the position and strength of the two major atmospheric surface pressure features in the Pacific Ocean, the Aleutian Low and Hawaiian High. That adjustment in surface atmospheric pressures projects onto surface winds, and the winds then modify the upper ocean, resulting in the anomalies observed in OSCAR current data. All of these results lend confidence to the conclusion that the MJO does project onto the upper ocean along the U.S. west coast on the intraseasonal time scale, particularly after tropical convection in the Indian Ocean and western Pacific Ocean. It is interesting that those two Phases (2 and 7) showed the strongest lagged differences, despite not being opposite each other in the RMM phase space. The physical mechanisms behind the differences between the atmospheric response to convection in the Indian Ocean versus the western Pacific Ocean are still being explored.

This intraseasonal variability is important for a wide array of physical and biological oceanography interests, including potential impacts on the timing, intensity, and duration of the spring bloom in the California Current system (Henson & Thomas, 2007). A follow-on study of biological impacts is planned. It is important to realize that there are also some limitations to the results in this study. For instance, the OSCAR product primarily captures geostrophic current variability in the upper 30 m of the ocean, and furthermore, the three-point horizontal spatial smoothing applied to the OSCAR data could have removed some of the signal for modulation of ocean mesoscale features. Hence, the results shown here likely most applicable to synoptic-scale features and geostrophic currents that are away from the immediate coastline. It is also important to note that no time lag between ocean currents and winds was explicitly considered, beyond the pentad time resolution of the OSCAR currents. Composite analysis was performed on standardized anomalies across four months, and it is possible that some smaller signals in months with smaller standard deviations could have been overweighted. Finally, given the strength and coherence of the signal in Phases 2 and 7, we recommend analyses of other data sets, such as high-frequency radar observations of the nearshore coastal environment, to further our understanding of the teleconnected ocean response to tropical atmospheric drivers like the MJO.

Acknowledgments
The OSCAR data were obtained from JPL Physical Oceanography DAAC and developed by ESR, available at ftp://podaac-ftp.jpl.nasa.gov/allData/oscar/preview/L4/oscar_third_deg/. The atmospheric reanalysis data were obtained from the ECMWF public data sets interface at http://www.ecmwf.int/en/research/climate-reanalysis/era-interim. The Real-time Multivariate MJO index was obtained from the Australian Bureau of Meteorology at http://www.bom.gov.au/climate/mjo/. This research was sponsored by NASA Physical Oceanography award NNX16AH61I.

References

Barrett, B. S., & Gensini, V. A. (2013). Variability of central United States April–May tornado day likelihood by phase of the Madden-Julian Oscillation. *Geophysical Research Letters*, *40*, 2790–2795. https://doi.org/10.1002/grl.50522

Barrett, B. S., Henderson, G. R., & Werling, J. S. (2015). The influence of MJO on the intraseasonal variability of Northern Hemisphere spring snow depth. *Journal of Climate*, *28*, 7250–7262.

Barrett, B. S., & Leslie, L. M. (2009). Links between the tropical cyclone activity and Madden-Julian Oscillation phase in the North Atlantic and Northeast Pacific basins. *Monthly Weather Review*, *137*, 727–744.

Barrett, B. S., & Raga, G. B. (2016). Variability of winter and summer surface ozone in Mexico City on the intraseasonal timescale. *Atmospheric Chemistry and Physics*, *16*, 15359–15370. https://doi.org/10.5194/acp-16-15359-2016

Baxter, S., & Nigam, S. (2013). A subseasonal teleconnection analysis: PNA development and its relationship to the NAO. *Journal of Climate*, *26*, 6733–6741. https://doi.org/10.1175/JCLI-D-12-00426.1

Baxter, S., Weaver, S., Gottschalck, J., & Xue, Y. (2014). Pentad evolution of wintertime impacts of the Madden–Julian Oscillation over the contiguous United States. *Journal of Climate*, *27*, 7356–7367. https://doi.org/10.1175/JCLI-D-14-00105.1

Biondi, F., Cayan, D., & Gershunov, A. (2001). North Pacific decadal climate variability since 1661. *Journal of Climate*, *14*, 5–10.

Bladé, I., & Hartmann, D. L. (1995). The linear and nonlinear extratropical response of the atmosphere to tropical intraseasonal heating. *Journal of the Atmospheric Sciences*, *52*, 4448–4471.

Bluestein, H. (1992). *Synoptic-dynamic meteorology in midlatitudes: Principles of kinematics and dynamics* (448 pp.). New York, NY: Oxford University Press.

Carlson, T. N. (1991). *Mid-latitude weather systems* (507 pp.). New York, NY: Harper Collins Academic.

Cassou, C. (2008). Intraseasonal interaction between the Madden–Julian oscillation and the North Atlantic Oscillation. *Nature*, *455*, 523–527. https://doi.org/10.1038/nature07286

Dee, D. P., Uppala, S. M., Simmons, A. J., Berrisford, P., Poli, P., Kobayashi, S., . . . Vitart, F. (2011). The ERA-Interim reanalysis: Configuration and performance of the data assimilation system. *Quarterly Journal of the Royal Meteorological Society*, *137*, 553–597. https://doi.org/10.1002/qj.828

Donald, A., Maia, A. de H. N., Meinke, H., Power, B., Stone, R. C., Wheeler, M. C., & White, N. (2006). Near global impact of the Madden-Julian oscillation on rainfall. *Geophysical Research Letters*, *33*, L09704. https://doi.org/10.1029/2005GL025155

Duvel, J. P., & Vialard, J. (2007). Indo-Pacific sea surface temperature perturbations associated with intraseasonal oscillations of tropical convection. *Journal of Climate*, *20*, 3056–3082.
Fauchereau, N. B., Pohl, A. & Lorrey, (2016). Extratropical impacts of the Madden–Julian Oscillation over New Zealand from a weather regime perspective. *Journal of Climate*, *29*, 2161–2175. https://doi.org/10.1175/JCLI-D-15-0152.1
Ferranti, L., Klinker, E., Molteni, F., & Palmer, T. N. (1990). Tropical-extratropical interaction associated with the 30–60 day oscillation and its impact on medium and extended range prediction. *Journal of the Atmospheric Sciences*, *47*, 2177–2199. https://doi.org/10.1175/1520-0469(1990)047<2177:TEIAWT>2.0.CO;2
Flatau, M., & Kim, Y. J. (2013). Interaction between the MJO and polar circulations. *Journal of Climate*, *26*, 3562–3574.
Goswami, B. N. (2005). South Asian summer monsoon. In W. K.-M. Lau & D. E. Waliser (Eds.), *Intraseasonal variability of the atmosphere-ocean climate system* (pp. 19–61). Berlin, Germany: Praxis Publishing.
Halkides, D. J., Guan, G., Menemenlis, D., Lee, T., & Waliser, D. E. (2015). Quantifying the processes controlling intraseasonal mixed-layer temperature variability in the tropical Indian Ocean. *Journal of Geophysical Research: Oceans*, *120*, 692–715. https://doi.org/10.1002/2014JC010139
Han, W. (2005). Origins and dynamics of the 90-day and 30–60-day variations in the equatorial Indian Ocean. *Journal of Physical Oceanography*, *35*, 708–728. https://doi.org/10.1175/JPO2725.1
Han, W., Lawrence, D. M., & Webster, P. J. (2001). Dynamical response of equatorial Indian Ocean to intraseasonal winds: Zonal flow. *Geophysical Research Letters*, *28*, 4215–4218. https://doi.org/10.1029/2001GL013701
Hasselmann, K., Barnett, T. P., Bouws, E., Carlson, H., Cartwright, D. E., Enke, K., . . . Walden, H. (1973). Measurements of wind-wave growth and swell during the Joint North Sea Wave Project (JONSWAP). *Deutsche Hydrographische*, *12*, 1–95.
Hendon, H. H. (2005). Air sea interaction. In *Intraseasonal variability in the atmosphere-ocean climate system* (pp. 223–246). Berlin, Germany: Praxis Publishing.
Hendon, H. H., Wheeler, M. C., & Zhang, C. (2007). Seasonal dependence of the MJO-ENSO relationship. *Journal of Climate*, *20*, 531–543.
Henson, S. A., & Thomas, A. C. (2007). Interannual variability in the timing of bloom initiation in the California Current System. *Journal of Geophysical Research*, *112*, C08007. https://doi.org/10.1029/2006JC003960
Hoskins, B. J., & Karoly, D. J. (1981). The steady linear response of a spherical atmosphere to thermal and orographic forcing. *Journal of the Atmospheric Sciences*, *38*, 1179–1196. https://doi.org/10.1175/1520-0469(1981)038<1179:TSLROA>2.0.CO;2
Iskandar, I., & McPhaden, M. J. (2011). Dynamics of wind-forced intraseasonal zonal current variations in the equatorial Indian Ocean. *Journal of Geophysical Research*, *116*, C06019. https://doi.org/10.1029/2010JC006864
Jin, F., & Hoskins, B. J. (1995). The direct response to tropical heating in a baroclinic atmosphere. *Journal of the Atmospheric Sciences*, *52*, 307–319. https://doi.org/10.1175/1520-0469(1995)052<0307:TDRTTH>2.0.CO;2
Jones, C., & Carvalho, L. M. V. (2014). Sensitivity to Madden–Julian Oscillation variations on heavy precipitation over the contiguous United States. *Atmospheric Research*, *147–148*, 10–26. https://doi.org/10.1016/j.atmosres.2014.05.002
Jones, C., Gautier, C., & Waliser, D. E. (1998). The influence of the Madden–Julian Oscillation on ocean surface heat fluxes and sea-surface temperatures. *Journal of Climate*, *11*, 1057–1072.
Kang, I. S., Ahn, M. S., Liu, F., Wang, B., & Yang, Y. M. (2013). The role of SST structure in convectively coupled Kelvin–Rossby waves and its implications for MJO formation. *Journal of Climate*, *26*, 5915–5930.
Kapur, A., & Zhang, C. (2012). Multiplicative MJO forcing of ENSO. *Journal of Climate*, *25*, 8132–8147.
Kemball-Cook, S., & Wang, B. (2001). Equatorial waves and air-sea interaction in the Boreal Summer Intraseasonal Oscillation. *Journal of Climate*, *14*, 2923–2942.
Klotzbach, P. J., & Oliver, E. C. J. (2015). Variations in global tropical cyclone activity and the Madden-Julian Oscillation since the midtwentieth century. *Geophysical Research Letters*, *42*, 4199–4209. https://doi.org/10.1002/2015GL063966
LaFleur, D. M., Barrett, B. S., & Henderson, G. R. (2015). Some climatological aspects of the Madden–Julian Oscillation (MJO). *Journal of Climate*, *28*, 6039–6053.
Latif, M., & Barnett, T. P. (1996). Decadal climate variability over the North Pacific and North America: Dynamics and predictability. *Journal of Climate*, *9*, 2407–2423.
L'Heureux, M. L., & Higgins, R. W. (2008). Boreal winter links between the Madden–Julian Oscillation and the Arctic Oscillation. *Journal of Climate*, *21*, 3040–3050. https://doi.org/10.1175/2007JCLI1955.1
Lin, H., & Brunet, G. (2009). The influence of the Madden–Julian Oscillation on Canadian wintertime surface air temperature. *Monthly Weather Review*, *137*, 2250–2262. https://doi.org/10.1175/2009MWR2831.1
Liu, C. X., Liu, Y., & Zhang, Y. L. (2015). Simulation of the Madden–Julian Oscillation in wintertime stratospheric ozone over the Tibetan Plateau and East Asia: Results from the specified dynamics version of the Whole Atmospheric Community Climate Model. *Atmospheric and Oceanic Science Letters*, *8*, 264–270.
Liu, X., Wang, J., Cheng, X., & Du, Y. (2012). Abnormal upwelling and chlorophyll *a* concentration off South Vietnam in summer 2007. *Journal of Geophysical Research*, *117*, C07021. https://doi.org/10.1029/2012JC008052
Madden, R. A., & Julian, P. R. (1972). Description of global-scale circulation cells in the tropics with a 40–50 day period. *Journal of the Atmospheric Sciences*, *29*, 1109–1123, https://doi.org/10.1175/1520-0469(1972)029<1109:DOGSCC>2.0.CO;2
Madden, R. A., & Julian, P. R. (1971). Detection of a 40–50 day oscillation in the zonal wind in the tropical Pacific. *Journal of the Atmospheric Sciences*, *28*, 702–708.
Madden, R. A., & Julian, P. R. (1994). Observations of the 40–50 day tropical oscillation: A review. *Monthly Weather Review*, *122*, 814–837.
Maloney, E. D., & Sobel, A. H. (2004). Surface fluxes and ocean coupling in the tropical intraseasonal oscillation. *Journal of Climate*, *17*, 4368–4386.
Marshall, A. G., & Hendon, H. H. (2014). Impacts of the MJO in the Indian Ocean and on the Western Australia coast. *Climate Dynamics*, *42*, 579–595.
Matthews, A. J., Hoskins, B. J., & Masutani, M. (2004). The global response to tropical heating in the Madden–Julian Oscillation during Northern winter. *Quarterly Journal of the Royal Meteorological Society*, *130*, 1991–2011.
Matthews, A. J., & Meredith, M. P. (2004). Variability of Antarctic circumpolar transport and the Southern Annular Mode associated with the Madden-Julian Oscillation. *Geophysical Research Letters*, *31*, L24312. https://doi.org/10.1029/2004GL021666
McPhaden, M. J. (1999). Genesis and evolution of the 1997–98 El Niño. *Science*, *283*, 950–954.
McWilliams, J. C., Moeng, C. H., & Sullivan, P. P. (1997). Langmuir turbulence in the ocean. *Journal of Fluid Mechanics*, *334*, 1–30.
Miles, J. W. (1957). On the generation of surface waves by shear flow, part I. *Journal of Fluid Mechanics*, *3*, 185–204.
Moum, J. N., de Szoeke, S. P, Smyth, W. D., Edson, J. B., DeWitt, H. L., Moulin, A. J., . . . Fairall, C. W. (2014). Air—sea interactions from westerly wind bursts during the November 2011 MJO in the Indian Ocean. *Bulletin of the American Meteorological Society*, *95*, 1185–1199, https://doi.org/10.1175/BAMS-D-12-00225.1

Phillips, O. M. (1985). Spectral and statistical properties of the equilibrium range in wind-generated gravity waves. *Journal of Fluid Mechanics*, *156*, 505–531.
Qiu, B. (2003). Kuroshio extension variability and forcing of the Pacific Decadal Oscillations: Responses and potential feedback. *Journal of Physical Oceanography*, *33*, 2465–2482.
Roundy, P. E. (2012). Tropical extratropical interactions. In *Intraseasonal variability in the atmosphere-ocean climate system* (pp. 497–512). Berlin, Germany: Praxis Publishing.
Roundy, P. E., & Kiladis, G. N. (2006). Observed relationships between oceanic Kelvin waves and atmospheric forcing. *Journal of Climate*, *19*, 5253–5272.
Sakaeda, N., & Roundy, P. E. (2015). The development of upper-tropospheric wind over the Western Hemisphere in association with MJO convective initiation. *Journal of the Atmospheric Sciences*, *72*, 3138–3160. https://doi.org/10.1175/JAS-D-14-0293.1
Sallee, J. B., Morrow, R., & Speer, K. (2008). Response of the Antarctic Circumpolar Current to atmospheric variability. *Journal of Climate*, *21*, 3020–3039.
Sardeshmukh, P. D., & Hoskins, B. J. (1988). The generation of global rotational flow by steady idealized tropical divergence. *Journal of the Atmospheric Sciences*, *45*, 1228–1251.
Schott, F. A., Xie, S.-P., & McCreary, J. P. Jr. (2009). Indian Ocean circulation and climate variability. *Reviews of Geophysics*, *47*, RG1002. https://doi.org/10.1029/2007RG000245
Sengupta, D., Senan, R., & Goswami, B. N. (2007). Intraseasonal variability of equatorial Indian Ocean zonal currents. *Journal of Climate*, *20*, 3036–3055.
Seo, H., Cavanaugh, N. R., Miller, A. J., & Subramanian, A. C. (2014). Coupled impacts of the diurnal cycle of sea surface temperature on the Madden–Julian Oscillation. *Journal of Climate*, *27*, 8422–8443.
Seo, K., & Son, S. (2012). The global atmospheric circulation response to tropical diabatic heating associated with the Madden–Julian Oscillation during northern winter. *Journal of the Atmospheric Sciences*, *69*, 79–96. https://doi.org/10.1175/2011JAS3686.1
Shinoda, T., Chen, S., Flatau, M., & Jensen, T. G. (2013). Surface wind and upper-ocean variability associated with the Madden–Julian Oscillation simulated by the Coupled Ocean-Atmosphere Mesoscale Prediction System (COAMPS). *Monthly Weather Review*, *141*, 2290–2307.
Shinoda, T., Kiladis, G. N., & Roundy, P. E. (2008). Variability of intraseasonal Kelvin waves in the equatorial Pacific Ocean. *Journal of Physical Oceanography*, *38*, 921–944.
Taylor, A. H., Jordan, M. B., & Stephens, J. A. (1998). Gulf Stream shifts following ENSO events. *Nature*, *393*, 638.
Waliser, D. E., Lucas, I. E., & Murtugudde, R. (2003). Indo-Pacific ocean response to atmospheric intraseasonal variability: 1. Austral summer and the Madden-Julian Oscillation. *Journal of Geophysical Research*, *108*(C5), 3160. https://doi.org/10.1029/2002JC001620
Wallace, J., & Gutzler, D. (1981). Teleconnections in the geopotential height field during the Northern Hemisphere winter. *Monthly Weather Review*, *109*, 784–812. https://doi.org/10.1175/1520-0493(1981)109<0784:TITGHF>2.0.CO;2
Wang, G., Ling, Z., Wu, R., & Chen, C. (2013). Impacts of the Madden–Julian Oscillation on the summer South China Sea ocean circulation and temperature. *Journal of Climate*, *26*, 8084–8096. https://doi.org/10.1175/JCLI-D-12-00796.1
Webber, B. G. M., Heywood, K. J., Matthews, A. J., & Stevens, D. P. (2012). Dynamical ocean forcing of the Madden–Julian Oscillation at lead times of up to five months. *Journal of Climate*, *25*, 2824–2842.
Webber, B. G. M., Matthews, A. J., & Heywood, K. J. (2010). A dynamical ocean feedback mechanism for the Madden–Julian Oscillation. *Quarterly Journal of the Royal Meteorological Society*, *136*(648), Part A, 740–754. https://doi.org/10.1002/qj.604
Weller, R. A., & Price, J. F. (1988). Langmuir circulation within the oceanic mixed layer. *Deep Sea Research, Part A*, *35*(5), 711–747.
Wheeler, M., & Hendon, H. H. (2004). An all-season real-time multivariate MJO index: Development of an index for monitoring and prediction. *Monthly Weather Review*, *132*, 1917–1932.
Woolnough, S. J., Balmaseda, M. A., & Vitart, F. (2007). The role of the oceans in Madden–Julian Oscillation: Impacts for MJO prediction. *Quarterly Journal of the Royal Meteorological Society*, *133*, 117–128.
Yamagata, T. (1985). Stability of a simple air-sea coupled model in the tropics. *Elsevier Oceanography Series*, *40*, 637–657.
Zhang, X., Lu, Y., & Thompson, K. R. (2010). Sea level variations in the tropical Pacific Ocean and the Madden–Julian Oscillation. *Journal of Physical Oceanography*, *39*, 1984–1992.
Zhou, L., & Murtugudde, R. (2010). Ocean-atmosphere coupling on different spatiotemporal scales: A mechanism for intraseasonal instabilities. *Journal of the Atmospheric Sciences*, *66*, 1834–1844.